water

MDPI

Article

Characteristics and Influence Rules of Roadside Ponding along the Qinghai–Tibet Highway

Fuqing Cui [1,2], Yu Zhu [1], Xiaona Liu [1], Jianbing Chen [2], Ke Mu [3] and Zhiyun Liu [1,*]

[1] College of Geology Engineering and Geomatics, Chang'an University, Xi'an 710054, China; cfq731@chd.edu.cn (F.C.); 2021126128@chd.edu.cn (Y.Z.); 2023226143@chd.edu.cn (X.L.)
[2] National Key Laboratory of Green and Long-Life Road Engineering in Extreme Environment, CCCC First Highway Consultants Co., Ltd., Xi'an 710065, China; chenjianbing@ccccltd.cn
[3] School of Management, Xi'an University of Finance and Economics, Xi'an 710100, China; muke@xaufe.edu.cn
* Correspondence: dcdgx33@chd.edu.cn; Tel.: +86-13484463421

Abstract: Due to climate change and seasonal precipitation, water conditions in the Qinghai–Tibet region are a significant factor affecting the stability of subgrades. The accumulation of large amounts of surface water leads to subgrade diseases along the Qinghai–Tibet Highway. Based on remote sensing photos obtained from Google Earth Engine and processing the photos using ENVI 5.6.3 and CAD 2019 software, this paper analyzed the distribution characteristics of surface water and studied the impact of roadside ponding on subgrade diseases. The results showed that the total area of surface water was more than 3.7 million m^2, and the surface water was most widely distributed in large river areas such as the Tuotuo River and Buqu River. The subgrade diseases of the Qinghai–Tibet Highway could be categorized into three types: settlement, longitudinal crack, and frost boiling, which accounted for 71.09%, 17.13%, and 11.78% of the total number of subgrade diseases, respectively. Additionally, the ground mean annual temperature was an important factor affecting the distribution of surface water, with the surface water area showing an increasing trend with the increase in ground mean annual temperature, and roadside ponding was most likely to form in the high-temperature extremely unstable permafrost area.

Keywords: Qinghai–Tibet Highway; roadside ponding; surface water; subgrade disease

Citation: Cui, F.; Zhu, Y.; Liu, X.; Chen, J.; Mu, K.; Liu, Z. Characteristics and Influence Rules of Roadside Ponding along the Qinghai–Tibet Highway. *Water* **2024**, *16*, 954. https://doi.org/10.3390/w16070954

Academic Editors: Jueyi Sui and Yuntong She

Received: 14 February 2024
Revised: 22 March 2024
Accepted: 23 March 2024
Published: 26 March 2024

1. Introduction

The Qinghai–Tibet Plateau is one of the few areas in the world with a large river network density [1–3], and the surface water along the Qinghai–Tibet Highway is widely distributed and densely populated [4–7]. The annual rainfall along the Qinghai–Tibet Highway is low but the rainfall season is relatively concentrated. Due to the lack of drainage facilities along the highway and the formation of soil pits on both sides in the early stage of road construction, part of the precipitation accumulates in low-lying areas on both sides of the highway, especially in the low mountain and hilly areas such as the Hoh Xili, Kaixinling and Wudaoliang Mountains [8,9]. In recent years, deterioration of the permafrost has intensified, and the ecological environment along the Qinghai–Tibet Highway has also undergone changes, resulting in frequent geological disasters.

The engineering problems caused by roadside ponding along the Qinghai–Tibet Highway are extremely complicated. Seasonal infiltration of surface water affects the stability of permafrost subgrades and changes in the internal moisture conditions of the subgrades lead to frost heave, overtopping, and other roadway diseases [10–14]. Mao et al. [15] investigated the road diseases of National Highway 109 on the Qinghai–Tibet Plateau and studied the impact of roadside ponding on the strength of Qinghai–Tibet Highway subgrades. They found that roadside ponding caused a decrease in the dynamic elastic modulus, which induced uneven deformation of the subgrades, longitudinal cracks, wave deformation, and other diseases. Wang et al. [16] established a permafrost subgrade model

on the Qinghai–Tibet Plateau based on the control equation of moisture and heat, and the results showed that water accumulation on the roadside had a significant effect on the deformation of subgrades, and longitudinal cracks were likely to be produced on the roadside where water had accumulated for a long period of time. Jiang [17] studied surface water accumulation in the Tuotuohe Basin by establishing a finite element model and found that the infiltration of surface water changed the volumetric water content of the subgrade, which in turn disturbed the thermal stability of perennial permafrost subgrades over time. Zhou [18] analyzed the change process of the temperature field of permafrost subgrades in the case of roadside ponding and determined that roadside ponding caused an uneven decrease in the upper limit of the permafrost in the subgrade, which led to an increase in the thawing depth of the subgrade.

The Qinghai–Tibet Plateau is known as the "Water Tower of Asia" due to its abundance of rivers, lakes, and glaciers [19–21], and climate change greatly affects the distribution of surface water in this region [22–25]. Luo et al. [26] developed a new method for high-precision surface water mapping based on Sentinel-1 synthetic aperture radar (SAR) images and convolutional networks (ConvNets) in order to obtain information on the dynamics of surface water in the Qinghai–Tibet Plateau region. Guan [27] explored the evolution trend of surface water resources on the Qinghai–Tibet Plateau based on multi-period remote sensing data, and the results showed that the surface of the Qinghai–Tibet Plateau as a whole tends to be wetter, and the trend of wetter changes in the central and western regions of the plateau was more significant. Ran et al. [28] established a dataset of surface water area on the Qinghai–Tibet Plateau from 2000 to 2020 and found that the average surface water area was about 59,481 km^2, with a significant increasing trend. Hu et al. [29] analyzed the water environment characteristics and influencing factors of highway roads in the Qinghai–Tibet Plateau region and found that rainfall runoff was an important influencing factor.

Existing studies have mainly analyzed the change characteristics of surface water area and the types of disease caused by roadside ponding, but they lack the analysis of influencing factors for surface water on the Qinghai–Tibet Highway, and the severity of diseases caused by roadside ponding is seldom involved [30–34]. Therefore, in order to study the distribution of surface water along the Qinghai–Tibet Highway and analyze the effect of roadside ponding on the subgrade, this paper investigated the surface water in the Qinghai–Tibet Engineering Corridor, conducted on-site surveys and monitored the typical lakes and ponds, and acquired 1059 high-magnitude remote sensing images along the Qinghai–Tibet Highway. This paper counted the area distribution of surface water in different sections of the Qinghai–Tibet Engineering Corridor and analyzed the surface water surface morphology to obtain the influence characteristics of ground mean annual temperature, ice content, and other factors on surface water of the Qinghai–Tibet Highway. By studying the relationship between roadside ponding on the Qinghai–Tibet Highway and permafrost subgrade diseases, the severity of different types of disease was analyzed to provide reference values for the maintenance of subgrade stability in the permafrost area.

2. Methods

2.1. Study Area

The Qinghai–Tibet Highway has a total length of 1147 km, crossing the permafrost area for about 550 km [35,36], and is densely populated with rivers along the route. The study area started from the Xidatan Fault Valley of the Qinghai–Tibet Highway in the north, near the northern boundary of the permafrost region of the Qinghai–Tibet Plateau Engineering Corridor, and ended at the Tanggula Mountains and intermountain basins in the south, near the southern boundary of the permafrost region of the Qinghai–Tibet Plateau Engineering Corridor. This study investigated and analyzed the surface water conditions on both sides of 14 areas along the Qinghai–Tibet Highway, as shown in Figure 1.

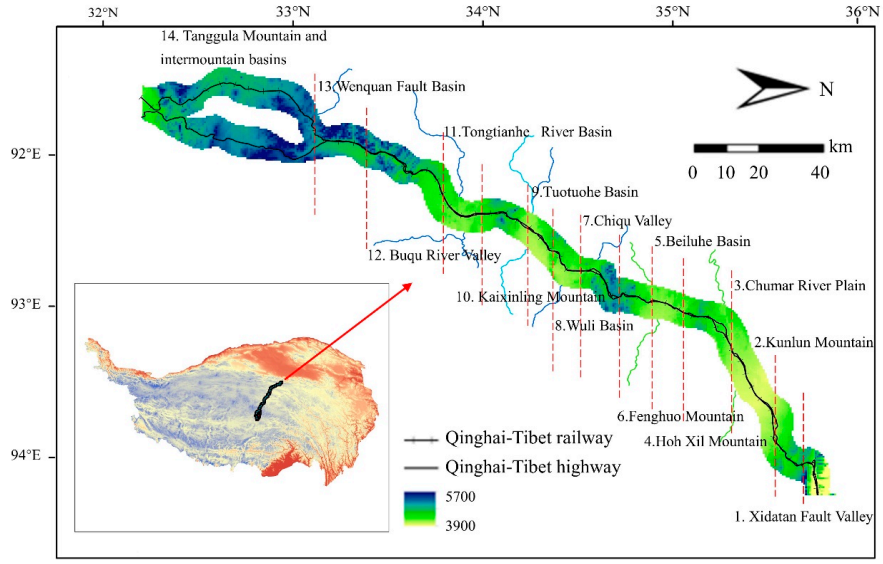

Figure 1. Study area along the Qinghai–Tibet Highway.

2.2. Data Source

Taking the Qinghai–Tibet Highway as the study center, Google Earth Engine (https://developers.google.cn/earth-engine/ accessed on 24 July 2014) was used to obtain a total of 1059 high-definition photographs along the left and right 300 m of the route, and the length of the highway was about 500 m for each photograph, which was a total highway mileage of about 540 km. Radiometric calibration and atmospheric correction of remote sensing photos were carried out with ENVI 5.6.3 (Environment for Visualizing Images) software, and the area of each surface water source point was calculated by CAD 2019 software. In addition, through on-site investigation, we also surveyed the water depth of typical lakes and ponds along the Qinghai–Tibet Highway and made a detailed investigation of the subgrade diseases along the route. Figure 2 presents examples of surface water in high-definition and on-site survey photographs.

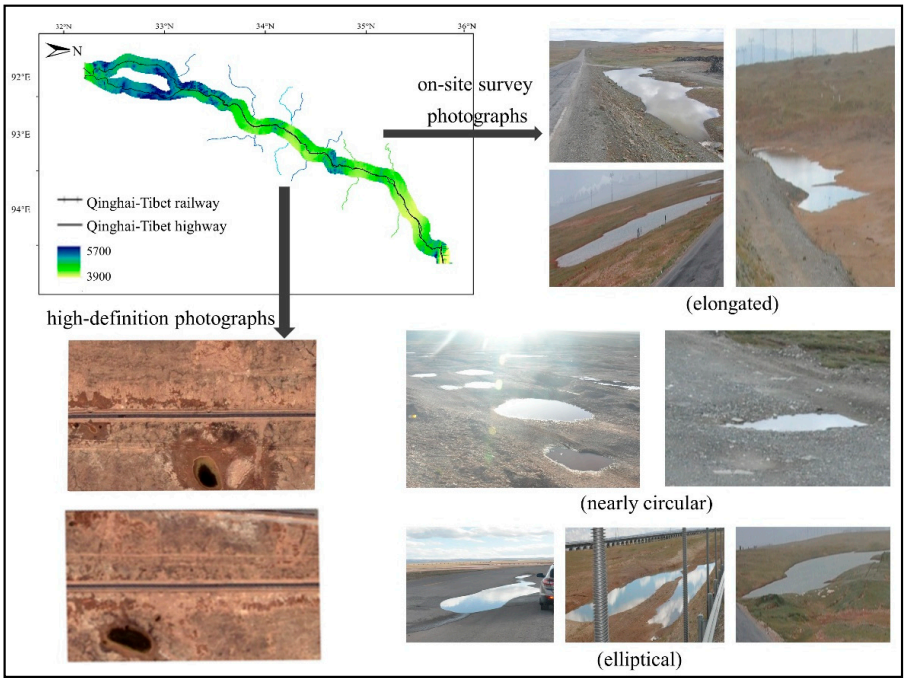

Figure 2. Photographs of surface water.

3. Results

3.1. Distribution Characteristics of Surface Water

Through statistically analyzing the source surface area of surface water along the Qinghai–Tibet Highway, it was found that the roadside surface water was richly distributed, totaling more than 3.7 million m^2. In order to study the distribution characteristics of surface water in various regions along the Qinghai–Tibet Highway, the distribution statistics of surface water in 14 sections along the highway are shown in Table 1.

Table 1. Regional distribution of surface water along the Qinghai–Tibet Highway.

Serial Number	Geomorphic Unit	Mileage	Number of Water Points	Total Area (m^2)	Number Within 10 m	Average Area (m^2)	Section Length (km)	Number of Water Points per Kilometer	Area per Kilometer (m^2/km)
1	Xidatan Fault Valley	K2866-K2877	16	1738	7	109	11	1.45	158
2	Kunlun Mountains	K2877-K2920	83	112,217	32	1662	43	1.93	2610
3	Chumar River Plain	K2920-K2982	137	221,393	36	1566	62	2.21	3571
4	Hoh Xil Mountains	K2982-K3035	23	79,663	5	3371	53	0.43	1503
5	Beiluhe Basin	K3035-K3056	23	139,924	1	6084	21	1.10	6663
6	Fenghuo Mountains	K3056-K3082	7	17,512	0	2190	26	0.27	674
7	Chiqu Valley	K3082-K3108	111	412,920	27	3720	26	4.27	15,882
8	Wuli Basin	K3108-K3127	51	158,810	4	9663	19	2.68	8358
9	Tuotuohe Basin	K3127-K3154	105	977,612	14	9311	27	3.89	36,208
10	Kaixinling Mountains	K3154-K3165	23	280,270	9	7607	21	2.09	25,479
11	Tongtianhe River Basin	K3165-K3190	39	104,422	2	2677	25	1.56	4177
12	Buqu River Valley	K3190-K3260	84	501,766	6	5973	70	1.20	7168
13	Wenquan Fault Basin	K3260-K3300	39	261,715	4	6711	40	0.98	6543
14	Tanggula Mountains and Intermountain Basins	K3300-K3420	181	502,391	21	2776	120	1.51	4187

As can be seen from Table 1, along the Qinghai–Tibet Highway, the Tanggula Mountains and intermountain basins had the largest number of surface water source points, with a total of 181. The Chumar River Plain, Chiqu Valley, and Tuotuo River Basin also had more than 100 surface water source points. And the Fenghuo Mountains had the scarcest surface water, with only seven water sources. From the perspective of surface water area, there was a large amount of surface water distributed in the Tuotuohe Basin and Buqu River Valley, with areas of 977,612 m^2 and 501,766 m^2, respectively. This indicated that surface water was widely distributed in large river basins along the Qinghai–Tibet Highway. In addition, the roadside surface water volume in the Kaixinling Mountains was also considerable, with an area of 280,270 m^2. From the frequency of surface water distribution, the surface water distribution in the Chumar River Plain, Chiqu Valley, Wuli Basin, and Tuotuohe Basin was relatively dense.

Through remote sensing image analysis along the Qinghai–Tibet Engineering Corridor, a total of 922 surface water sources were identified, including 170 Talik and 752 permafrost regions. The area distribution is shown in Figure 3. As shown in the figure, the surface water area was mainly distributed in the range of 1000~10,000 m^2, in which the inner Talik and permafrost regions accounted for 65.5% and 66.2%, respectively, indicating that the distribution characteristics of the two types of areas were basically similar.

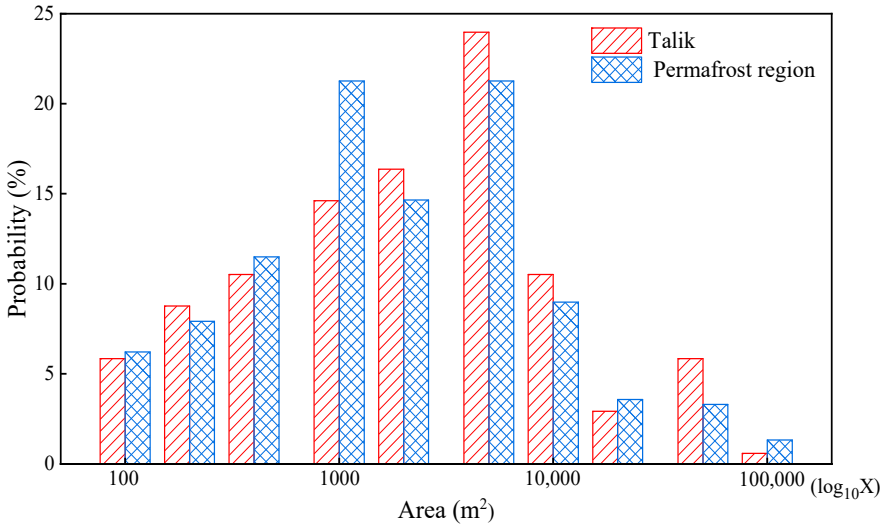

Figure 3. Area distribution of surface water along the Qinghai–Tibet Highway.

According to the ratio of the long and short axes of surface water sources, the water surface morphology was divided into three categories: nearly circular (1–2), elliptical (2–4), and elongated (>4). The statistical results of the surface water morphology along the Qinghai–Tibet Highway are shown in Figure 4. It can be seen from the probability distribution that the surface water morphology along the Qinghai–Tibet Highway showed a significant downward trend with the increase in the ratio of the long and short axes. The proportions of the three types of surface water morphology, nearly circular, elliptical, and long strip, were 53.5%, 32.5%, and 14%, respectively. Therefore, the surface water morphology along the Qinghai–Tibet Highway was basically nearly circular.

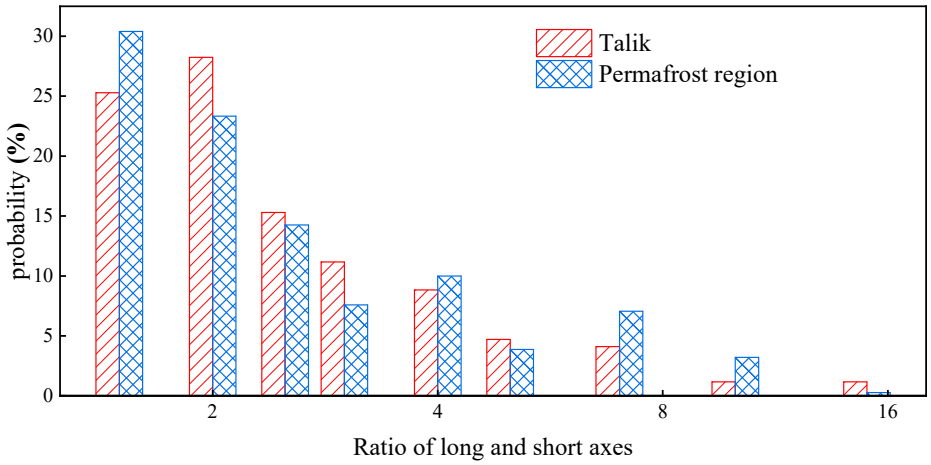

Figure 4. Distribution of surface water morphology along the Qinghai–Tibet Highway.

3.2. Analysis of Typical Lakes and Ponds

Due to climate warming and permafrost melting, there are a large number of thermally melted lakes and ponds around the Qinghai–Tibet Highway. In order to further analyze the roadside surface water characteristics of the Qinghai–Tibet Highway, this study conducted field investigation and testing of typical surface water along the route and conducted related tests on the water depth of each lake and pond. The results are shown in Table 2. As can be seen from the table, there was no obvious correlation between surface water area and water depth along the Qinghai–Tibet Highway, and the depth of surface water was relatively shallow, generally below 1 m.

Table 2. Statistics of typical lakes and ponds along the Qinghai–Tibet Highway.

Serial Number	Mileage	Longitude	Latitude	Water Depth/cm	Area/m^2
1	K2925 + 300	93°51′01	35°30′52	92	2365
2	K2949 + 100	93°37′16	35°27′12	202	6224
3	K2958 + 100	93°32′44	35°24′07	71	16,356
4	K2959 + 600	93°31′46	35°23′47	39	3996
5	K2961 + 500	93°30′28	35°23′17	81	15,703
6	K2964 + 500	93°29′00	35°22′40	21	19,740
7	K2968 + 100	93°26′40	35°21′57	17	5947
8	K2972 + 200	93°23′51	35°21′27	25	4011
9	K2979 + 100	93°20′00	35°19′57	201	1365
10	K2994 + 000	93°11′51	35°16′06	55	1527
11	K3041 + 000	92°57′16	34°57′26	72	25,433
12	K3050 + 200	92°56′09	34°52′37	22	989
13	K3052 + 900	92°56′57	34°51′17	27	1351
14	K3056 + 500	92°55′47	34°49′01	63	2415
15	K3057 + 500	92°55′59	34°49′19	94	852
16	K3079 + 700	92°54′03	34°39′09	56	1274
17	K3085 + 100	92°51′14	34°37′52	66	2448
18	K3095 + 500	92°45′12	34°35′44	94	1504
19	K3107 + 500	92°43′45	34°29′25	53	1790
20	K3110 + 200	92°29′24	34°16′55	92	10,702
21	K3128 + 000	92°32′09	34°18′21	32	11,420
22	K3140 + 000	92°36′11	34°22′32	81	59,044
23	K3145 + 000	92°43′42	34°27′57	173	8452

3.3. Impact of Roadside Ponding on Subgrade Diseases

3.3.1. Statistics of Subgrade Diseases along the Qinghai–Tibet Highway

In this study, a large number of subgrade diseases in the permafrost area of the Qinghai–Tibet Highway were investigated. The subgrade diseases of the Qinghai–Tibet Highway were mainly divided into three categories, namely settlement, longitudinal crack, and frost boiling. Settlement is mainly caused by the uneven settlement of the subgrade, which will seriously affect the bearing capacity of the road surface and accelerate the destruction of pavement mechanism. Longitudinal crack is caused by the capillary phenomenon at the bottom of the subgrade, caused by water on both sides of the subgrade, and uneven settlement or unilateral sliding on both sides of the highway after freeze and thaw cycles. Similarly, due to the existence of water under the pavement structure, the occurrence of freeze–thaw cycles lead to the reduction of local bearing capacity, which presses the pavement structure under the action of load and produces the phenomenon of frost boiling. In order to analyze the characteristics of subgrade diseases in different regions along the Qinghai–Tibet Highway, the types of disease in each region were statistically analyzed, as shown in Figure 5.

As can be seen from Figure 5, subgrade settlement disease was the main type of disease along the Qinghai–Tibet Highway, and there were different distribution characteristics of subgrade disease in different sections. The Tanggula Mountains and intermountain basins had the largest number of overall diseases, and the number of settlement, longitudinal crack, and frost boiling diseases were the highest among all regions, reaching 72, 25, and 22, respectively. The Kaixinling Mountains had the lowest number of diseases, with only three subgrade settlement diseases along the road. From the perspective of different disease types, in addition to the main distribution of diseases in the Tanggula Mountains and intermountain basins, the subgrade settlement diseases of the Qinghai–Tibet Highway were mainly distributed in the Chumar River Plain, Kunlun Mountains, and Buqu River Valley, and the number of diseases in these sections was more than 30. Longitudinal crack was mainly distributed in the Chumar River Plain and Tongtianhe Basin, where the number of diseases reached 10 or more, and in the Beiluhe Basin, there were also 8 longitudinal

cracks. The number of frost boilings in the Chumar River Plain region was 9, and the number of diseases in other regions was below 5.

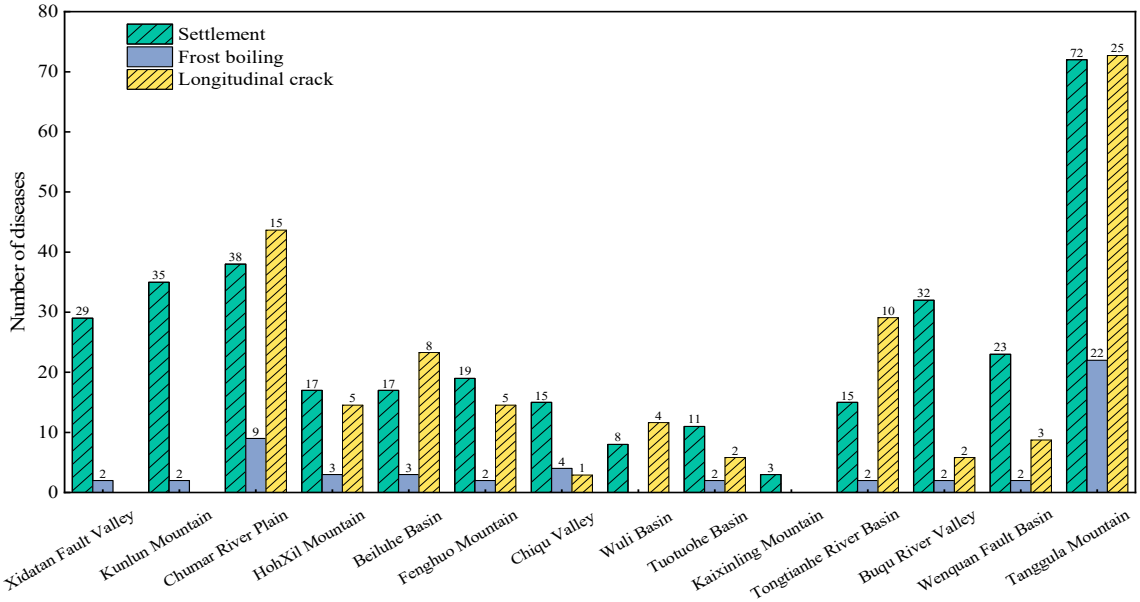

Figure 5. Statistics of subgrade disease types in each section.

3.3.2. Subgrade Disease Severity Analysis

According to the severity of subgrade diseases along the Qinghai–Tibet Highway, they could be divided into severe (heavy), moderate (medium), and slight (light). A total of 467 subgrade diseases along the Qinghai–Tibet Highway were statistically analyzed under conditions of roadside ponding and no roadside ponding, and the analysis results are shown in Figure 6. As can be seen from Figure 6, the number of subgrade diseases along the Qinghai–Tibet Highway was high, mainly presenting the disease forms of settlement and longitudinal crack, and the severity of longitudinal crack produced by the subgrade was overall high.

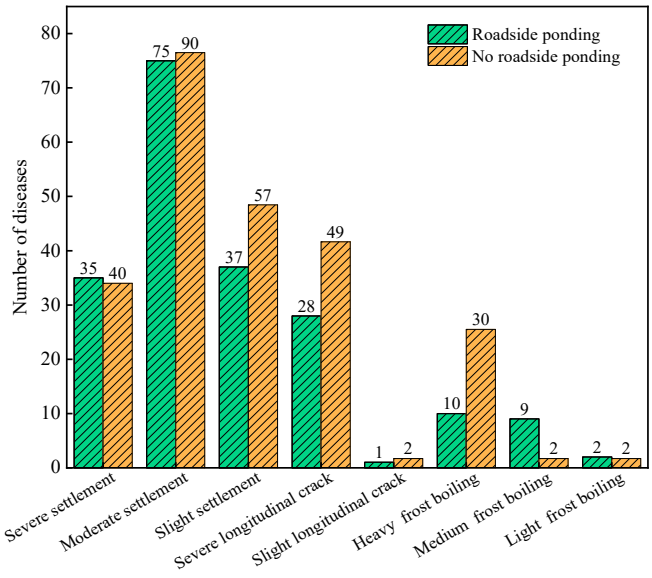

Figure 6. Disease analysis results of the Qinghai–Tibet Highway.

In the case of the Qinghai–Tibet Highway with or without roadside ponding, the disease rates were calculated respectively, and the relationship between disease rate and

roadside ponding of different types of permafrost subgrade was obtained, as shown in Figure 7. It can be seen from the figure that the disease rates of sections with roadside ponding were significantly higher than those without water accumulation, indicating that roadside ponding had a strong correlation with the generation and development of permafrost subgrade diseases. Among the three types of Qinghai–Tibet Highway subgrade diseases, roadside ponding had a significant impact on the incidence of road settlement. In the case of roadside ponding, the rate of road settlement disease was about twice that without roadside ponding. This was due to surface water seeping into the highway foundation, reducing the bearing capacity of the foundation and the shear strength of the foundation materials, resulting in subgrade settlement. Moreover, the permafrost hydrothermal coupling process was affected and the subgrade was subjected to lateral thermal erosion, leading to temperature rise and settlement.

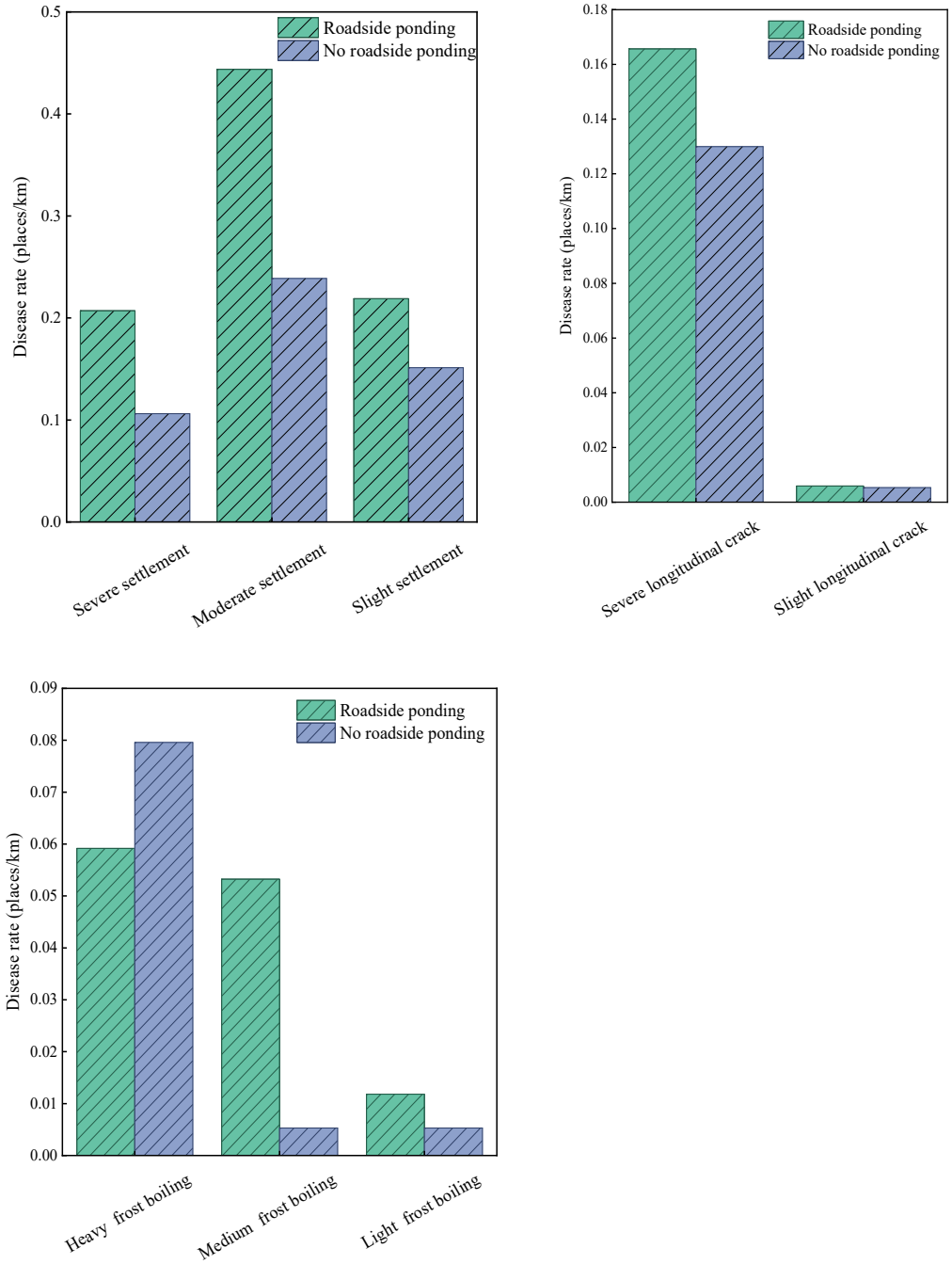

Figure 7. Disease rate of Qinghai–Tibet Highway with or without roadside ponding.

In the case of roadside ponding along the Qinghai–Tibet Highway, the minimum distance from the water accumulation point to the foot of the subgrade slope was calculated, and its proportion to the total disease is shown in Figure 8. From the figure, it can be seen that both the total proportion and the proportion of diseases with different severity levels showed an increasing trend as the minimum distance from the roadside ponding point to the foot of the subgrade slope decreased, and the trend became more obvious with decreased distance. When the distance exceeded 30 m, the relationship between the minimum distance of the roadside ponding point and its disease was not very obvious, indicating that the distance between the roadside ponding and the permafrost subgrade was about 30 m.

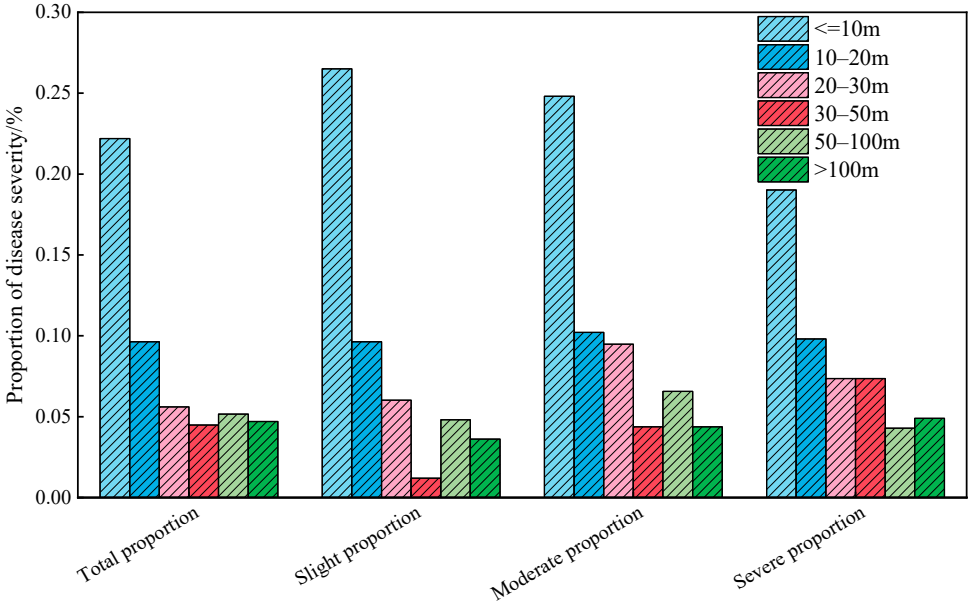

Figure 8. Proportion of different distances to total diseases in roadside ponding areas.

4. Discussion

4.1. The Influence of Ground Mean Annual Temperature

Due to global warming and climate change, the ground temperature in the Qinghai–Tibet region showed an increasing trend. Statistics on surface water in different ground mean annual temperature (GMAT) regions in the Qinghai–Tibet Engineering Corridor were obtained, and the distribution characteristics of surface water sources along the route are shown in Table 3. It can be seen from the table that the surface water source area in the high-temperature extremely unstable permafrost area ($-0.5 \leq$ GMAT < 0 °C) was the largest, reaching 1.63 million m^2. This was because the existence of the perennial permafrost layer as a water insulation layer made the infiltration of surface water difficult, which created the gathering of a large amount of surface water.

Table 3. Distribution characteristics of surface water sources in different GMAT.

Ground Mean Annual Temperature/°C	Surface Water Source Points		Surface Water Source Area		Permafrost Distribution	
	Count	Proportion (%)	Area (10^4 m^2)	Proportion (%)	Length (km)	Proportion (%)
GMAT < -1.5	205	22.21	33.04	9.24	112	20.6
$-1.5 \leq$ GMAT < -0.5	360	39.00	97.62	27.30	139	25.6
$-0.5 \leq$ GMAT < 0	187	20.26	163.07	45.61	149	27.5
Talik	171	18.53	63.84	17.85	142	26.2

Statistical analysis of the ground mean annual temperature area probability distribution of surface water along the Qinghai–Tibet Highway is shown in Figure 9. It can be seen

that in the high-temperature extremely unstable permafrost area (−0.5 ≤ GMAT < 0 °C), surface water exhibited the characteristics of fewer water source points but larger water area. This was because compared to the high-temperature unstable permafrost area (−1.5 ≤ GMAT < −0.5 °C) and low-temperature stable and basically stable permafrost area (GMAT < −1.5 °C), the active layer thickness of the high-temperature extremely unstable permafrost area (−0.5 ≤ GMAT < 0 °C) was larger and the impermeable layer was deeper, resulting in small areas of water sources that easily infiltrated and dissipated, making it difficult to maintain.

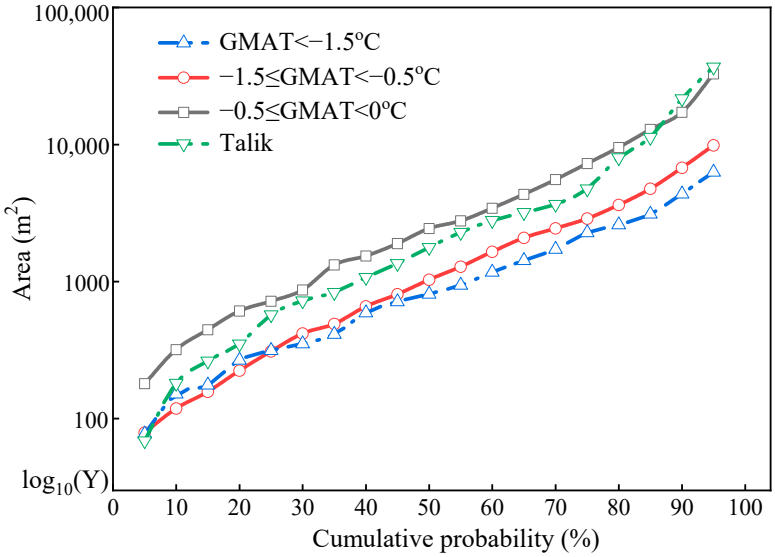

Figure 9. Area probability distribution of ground mean annual temperature.

4.2. The Influence of Ice Content

According to the statistics of surface water in permafrost areas with different ice contents in the Qinghai–Tibet Engineering Corridor, the distribution characteristics of surface water sources are shown in Table 4. It can be seen from the table that with the increase in ice content, the surface water volume increased. Among them, the ice-poor/icy soil permafrost region accounted for more than 40% of the total section length, but the proportion of surface water points along the route side was only 9.44% and its area proportion was only 7.72%. It was considered that the roadside surface water of the section with less ice content was obviously lower than that of the section with large ice content. Figure 10 shows the probability distribution of ice content in the permafrost area. From the unit area distribution of surface water source points, ice content had no significant impact on the area of water source points. The area of water source points with ice-poor/icy soil permafrost was even higher than that of the area with ice layer with soil inclusions.

Table 4. Distribution characteristics of surface water sources in different ice content.

Type of Ice Content	Surface Water Source Points		Surface Water Source Area		Permafrost Distribution	
	Count	Proportion (%)	Area (10^4 m^2)	Proportion	Length (km)	Proportion (%)
Ice-poor/Icy soil	87	9.44	21.38	7.72	164	41.04
Ice-rich/Ice-saturated	442	47.94	179.22	64.72	86	21.44
Ice layer with soil inclusions	233	25.27	76.3	27.56	150	37.52

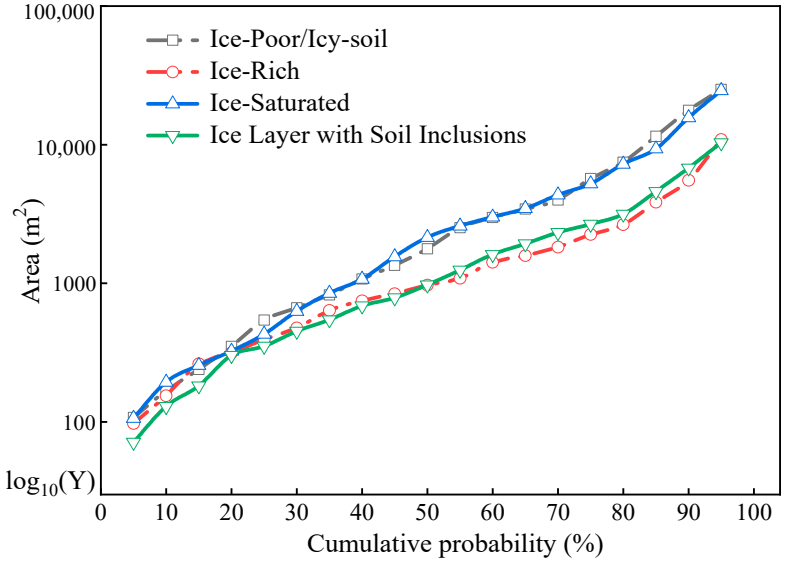

Figure 10. Area probability distribution of ice content.

4.3. The Influence of Highway Construction

The distance and water source points between the roadside surface water and the foot of the Qinghai–Tibet Highway slope were statistically analyzed, and the results are shown in Figure 11. It can be seen that most of the water source points along the Qinghai–Tibet Highway were close to the highway, and the number of roadside surface water source points decreased sharply as the distance increased. This indicated that the construction of the Qinghai–Tibet Highway had a significant promoting effect on the destruction of natural surface water and the formation of roadside surface water. Consistent with the previous analysis of the impact of ground mean annual temperature, as the ground temperature increased, the proportion of surface water formed due to the influence of highway construction correspondingly decreased, indicating that low-temperature permafrost areas were more susceptible to the influence of highway construction and formation of roadside surface water.

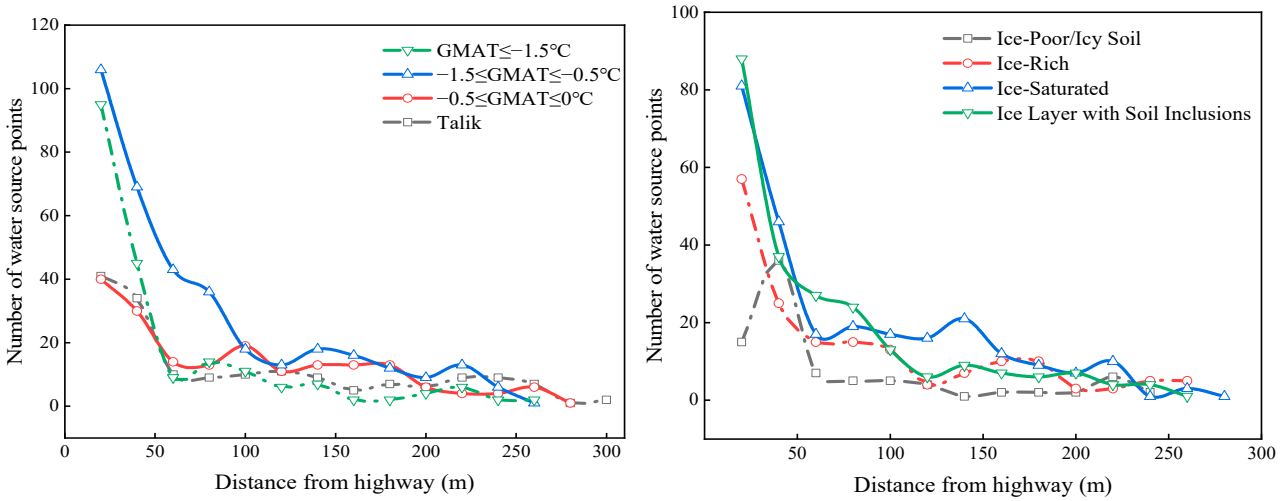

Figure 11. Distribution of surface water distance and water source points.

Meanwhile, it can also be seen from Figure 11 that when the distance from the highway exceeded 100 m, its impact basically disappeared. To further analyze the impact of different distances between surface water and the highway, the probability distribution of surface water source areas in different intervals with road distances of <30 m, 30–100 m, and >100 m

was calculated, as shown in Figure 12. It can be seen that the probability distribution of surface water source point areas was basically the same within 100 m, but the area increased significantly after exceeding 100 m. It was considered that the impact of highways disappeared after 100 m, and the area mainly consisted of naturally formed lakes and ponds, and their average area increased accordingly.

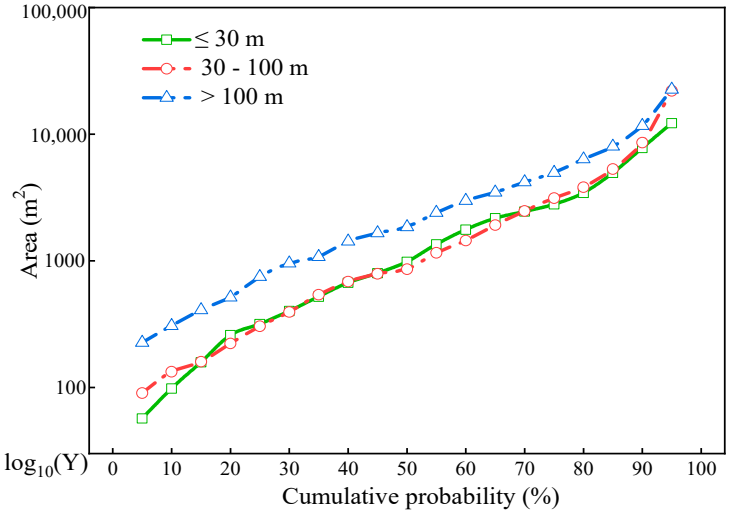

Figure 12. Distribution of surface water distance from the highway and water source area.

In addition, statistical analysis was conducted on the distance between the surface water morphology and the highway, and the probability distribution is shown in Figure 13. It can be seen from the figure that the probability distribution of the distance from the highway of the nearly circular or elliptical surface water was basically the same, with mean values of 74.55 m and 75.18 m, respectively. The elongated morphology was obviously closer to the highway, with a mean value of 38.04 m, and it was basically distributed near the highway area, with 50% of surface water within 22 m and 80% of surface water within 50 m. The long axis direction of surface water was basically consistent with the direction of the highway, which further indicated that the highway had a strong influence on the formation of roadside surface water.

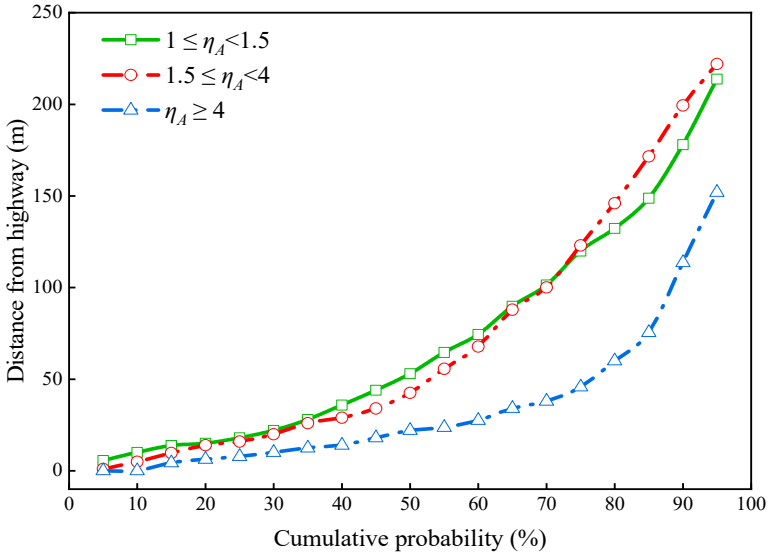

Figure 13. Cumulative probability distribution of distance between different surface water morphologies and the Qinghai–Tibet Highway.

5. Conclusions

The Qinghai–Tibet Plateau has high terrain and a cold climate, and changes in climate and precipitation have an impact on the subgrade. Based on field survey and remote sensing data along the Qinghai–Tibet Engineering Corridor, this paper analyzed the distribution characteristics of surface water and its influencing factors and studied the impacts of roadside ponding on subgrade diseases. The following conclusions can be drawn from the study results:

(1) Surface water was widely distributed along the Qinghai–Tibet Highway, with the Tuotuohe Basin and Buqu River Valley having the largest surface water areas of 977,612 m^2 and 501,766 m^2, respectively. In addition, the Chumar River Plain, Chiqu Valley, and Wuli Basin also had abundant surface water sources.

(2) The subgrade diseases of the Qinghai–Tibet Highway can be divided into three categories, settlement, longitudinal crack, and frost boiling, which accounted for 71.09%, 17.13%, and 11.78% of the total number of subgrade diseases, respectively. The disease rate in the road section with roadside ponding was significantly higher than that in the section without roadside ponding.

(3) The ground annual mean temperature, ice content, and road construction all had an impact on the roadside surface water of the Qinghai–Tibet Highway. As the ground annual mean temperature and ice content of the permafrost increased, the surface water area showed an increasing trend. The construction of highways had a strong promoting effect on the formation of roadside surface water.

Author Contributions: Conceptualization, F.C. and Y.Z.; methodology, X.L.; software, F.C. and K.M.; validation, Y.Z., X.L. and J.C.; formal analysis, X.L. and Z.L.; investigation, Y.Z.; resources, F.C. and K.M.; data curation, J.C. and Z.L.; writing—original draft preparation, F.C.; writing—review and editing, Y.Z.; visualization, X.L.; supervision, K.M.; project administration, J.C.; funding acquisition, F.C. and Z.L. All authors have read and agreed to the published version of the manuscript.

Funding: This research was funded by the National Science Foundation of China (Grant No. 42371149, 42230712), the Natural Science Foundation of Shaanxi Province (Grant No. 2022JM-143), the open fund of the National Key Laboratory of Green and Long-Life Road Engineering in Extreme Environment (YGY2021KFKT03), and the Scientific Innovation Practice Project of Postgraduates of Chang'an University (300103723048). We are grateful to the anonymous reviewers for their constructive comments to improve this manuscript.

Data Availability Statement: The data are available in the case that they are required.

Conflicts of Interest: Author Jianbing Chen was employed by the company National Key Laboratory of Green and Long-Life Road Engineering in Extreme Environment, CCCC First Highway Consultants Co., Ltd. The remaining authors declare that the research was conducted in the absence of any commercial or financial relationships that could be construed as a potential conflict of interest.

References

1. Guo, X.W.; Gao, P.; Li, Z.W. Morphological characteristics and changes of two meandering rivers in the Qinghai-Tibet Plateau, China. *Geomorphology* **2021**, *379*, 107626. [CrossRef]
2. Pan, Y.X.; Sun, Z.Y.; Pan, Z.; Zhang, S.X.; Li, X.; Ma, R. Influence of permafrost and hydrogeology on seasonal and spatial variations in water chemistry of an alpine river in the north-eastern Qinghai-Tibet Plateau, China. *Sci. Total Environ.* **2022**, *834*, 155227. [CrossRef] [PubMed]
3. Qin, C.; Wu, B.S.; Wang, G.Q.; Wang, G. Spatial Distributions of At-Many-Stations Hydraulic Geometry for Mountain Rivers Originated from the Qinghai-Tibet Plateau. *Water Resour. Res.* **2021**, *57*, e2020WR029090. [CrossRef]
4. Wan, W.; Xiao, P.F.; Feng, X.Z.; Li, H.; Ma, R.H.; Duan, H.T.; Zhao, L.M. Monitoring lake changes of Qinghai-Tibetan Plateau over the past 30 years using satellite remote sensing data. *Chin. Sci. Bull.* **2014**, *59*, 1021–1035. [CrossRef]
5. Chen, F.; Zhang, M.M.; Tian, B.S.; Li, Z. Extraction of Glacial Lake Outlines in Tibet Plateau Using Landsat 8 Imagery and Google Earth Engine. *IEEE J. Sel. Top. Appl. Earth Obs. Remote Sens.* **2017**, *10*, 4002–4009. [CrossRef]
6. Chen, X.; Wang, G.L.; Wang, F.Q. Classification of Stable Isotopes and Identification of Water Replenishment in the Naqu River Basin, Qinghai-Tibet Plateau. *Water* **2019**, *11*, 46. [CrossRef]

7. Liu, W.X.; Zhang, H.; Liu, Y.; Lu, H.J.; Guo, C.S.; Xu, J. Occurrence, distribution, and ecological risk of psychoactive substances in typical lakes and rivers in Qinghai-Tibet Plateau. *Ecotoxicol. Environ. Saf.* **2022**, *242*, 113928. [CrossRef] [PubMed]
8. Wang, X.X.; Xiao, X.M.; Zou, Z.H.; Dong, J.W.; Qin, Y.W. Gainers and losers of surface and terrestrial water resources in China during 1989–2016. *Nat. Commun.* **2020**, *11*, 3471. [CrossRef] [PubMed]
9. Tao, S.L.; Fang, J.Y.; Zhao, X.; Zhao, S.Q.; Shen, H.H.; Hu, H.F.; Tang, Z.Y.; Wang, Z.H.; Guo, Q.H. Rapid loss of lakes on the Mongolian Plateau. *Proc. Natl. Acad. Sci. USA* **2015**, *112*, 2281–2286. [CrossRef] [PubMed]
10. Pritchard, H.D. Asia's shrinking glaciers protect large populations from drought stress. *Nature* **2019**, *569*, 649–654. [CrossRef]
11. Zhang, G.Q.; Yao, T.D.; Piao, S.L.; Bolch, T.; Xie, H.G. Extensive and drastically different alpine lake changes on Asia's high plateaus during the past four decades. *Geophys. Res. Lett.* **2017**, *44*, 252–260. [CrossRef]
12. Wu, R.Z.; Liu, G.X.; Zhang, R.; Wang, X.W.; Li, Y.; Zhang, B.; Cai, J.L.; Xiang, W. A deep learning method for mapping glacial lakes from the combined use of synthetic-aperture radar and optical satellite images. *Remote Sens.* **2020**, *12*, 4020. [CrossRef]
13. Hou, Z.J.; Mao, X.S.; Ma, G. Testing and Analysis of Strength Performance of Qinghai Tibet Highway Roadbed. *Roadbed Eng.* **2007**, *1*, 55–56.
14. Cui, X.Z.; Li, X.Y.; Du, Y.F.; Bao, Z.H.; Zhang, X.N.; Hao, J.W.; Hu, Y.Y. Macro-micro numerical analysis of granular materials considering principal stress rotation based on DEM simulation of dynamic hollow cylinder test. *Constr. Build. Mater.* **2024**, *412*, 134818. [CrossRef]
15. Mao, X.S.; Ling, S.D.; Zhang, Z.B. Analysis of the influence of roadside waterlogging on the strength of Qinghai Tibet Highway subgrade. *J. Wuhan Univ. Technol. Transp. Sci. Eng. Ed.* **2013**, *37*, 456–459.
16. Wang, N.; Meng, Q.M.; Yang, J.F. The Numerical Analysis of Roadside Water Effects on Qinghai-Tibet Highway Sub-Grade Longitudinal Cracks. *Appl. Mech. Mater.* **2014**, *505*, 168–173. [CrossRef]
17. Jiang, L.K. Numerical Study on the Influence of Surface Water on the Temperature of a Permafrost Foundation in a Certain Year. Master's Thesis, Lanzhou Jiaotong University, Lanzhou, China, 2023. [CrossRef]
18. Zhou, L.J. Numerical analysis of the influence of roadside waterlogging on the temperature field of roadbed in permafrost areas. *North. Transp.* **2015**, *8*, 43–46. [CrossRef]
19. Immerzeel, W.W.; Van, B.L.; Bierkens, M.F.P. Climate change will affect the Asian water towers. *Science* **2010**, *328*, 1382–1385. [CrossRef] [PubMed]
20. Kong, W.M.; Wei, M.D.; Hu, Y.K. Current situation and future estimation of water resource pressure in the "Asian Water Tower" basin under the background of temperature rise. *Glacier Permafr.* **2023**, *1*, 12. Available online: http://kns.cnki.net/kcms/detail/62.1072.P.20230322.2315.008.html (accessed on 16 February 2023).
21. Xu, X.D.; Dong, L.L.; Zhao, Y.; Wang, Y.J. Effect of the Asian Water Tower over the Qinghai-Tibet Plateau and the characteristics of atmospheric water circulation. *Chin. Sci. Bull.* **2019**, *64*, 2830–2841. [CrossRef]
22. Connor, R. *The United Nations World Water Development Report 2015: Water for a Sustainable World*; UNESCO Publishing: Paris, France, 2015. [CrossRef]
23. Tulbure, M.G.; Broich, M.; Stehman, S.V.; Kommareddy, A. Surface water extent dynamics from three decades of seasonally continuous Landsat time series at subcontinental scale in a semi-arid region. *Remote Sens. Environ.* **2016**, *178*, 142–157. [CrossRef]
24. Qiao, B.J.; Zhu, L.P.; Yang, R.M. Temporal-spatial differences in lake water storage changes and their links to climate change throughout the Tibetan Plateau. *Remote Sens. Environ.* **2019**, *222*, 232–243. [CrossRef]
25. Li, Y.K.; Liao, J.J.; Guo, H.D.; Liu, Z.W.; Shen, G.Z. Patterns and potential drivers of dramatic changes in Tibetan lakes, 1972–2010. *PLoS ONE* **2014**, *9*, e111890. [CrossRef]
26. Luo, X.; Hu, Z.W.; Liu, L. Investigating the seasonal dynamics of surface water over the Qinghai–Tibet Plateau using Sentinel-1 imagery and a novel gated multiscale ConvNet. *Int. J. Digit. Earth* **2023**, *16*, 1372–1394. [CrossRef]
27. Guan, Y.L. Study on the Change of Global Climate Landscape Pattern and Its Impact on Surface Water Resources in Tibetan Plateau. Ph.D. Thesis, North China Electric Power University, Beijing, China, 2021. [CrossRef]
28. Ran, Q.W.; Aires, F.; Ciais, P.; Qiu, C.J.; Hu, R.H.; Fu, Z.; Xue, K.; Wang, Y.F. The Status and Influencing Factors of Surface Water Dynamics on the Qinghai-Tibet Plateau During 2000–2020. *IEEE Trans. Geosci. Remote Sens.* **2022**, *61*, 4200114. [CrossRef]
29. Hu, L.; Wang, Q.; Shan, Y.T. The water environment characteristics of typical highway areas in the Qinghai Tibet Plateau region. *Soil Water Conserv. Bull.* **2017**, *37*, 286–291. [CrossRef]
30. Shun, B.L.; Qing, S.; Bao, Y.H. The spatiotemporal changes and influencing factors of surface water area in Inner Mongolia from 2009 to 2018. *Soil Water Conserv. Bull.* **2021**, *41*, 312–319. [CrossRef]
31. Cao, S.K.; Cao, G.C.; Wang, Z.G.; Hou, Y.F.; Wang, Y.C.; Kang, L.G. Isotopic hydrological links among precipitation, river water and groundwater in an alpine mountain basin, NE Qinghai-Tibet Plateau in warm seasons. *Environ. Earth Sci.* **2022**, *81*, 366. [CrossRef]
32. Zhou, S.R.; Xin, Z.B. Spatial and temporal changes of water resources in the Qinghai Tibet Plateau over the past 20 years. *J. Yangtze River Acad. Sci.* **2022**, *39*, 31–39. [CrossRef]
33. Yang, J.F. Research on the Influence of Hydrothermal Changes on Longitudinal Cracks in Roadbeds of Qinghai Tibet Highway. Ph.D. Thesis, Chang'an University, Xi'an, China, 2014.
34. Zhao, W.T.; Cheng, Y.Z.; Jian, J.S.; Jiao, J.Y.; Cheng, C.W.; Li, J.J.; Chen, T.D. Water erosion changes on the Qinghai-Tibet Plateau and its response to climate variability and human activities during 1982–2015. *Catena* **2023**, *229*, 107207. [CrossRef]

35. Jiao, S.H.; Wang, L.Y.; Liu, G.G. Prediction of Distribution Changes of Permafrost on the Qinghai Tibet Plateau under the Background of Global Warming. *J. Peking Univ. (Nat. Sci. Ed.)* **2016**, *52*, 249–256. [CrossRef]
36. Zhou, B.; Wei, G.; Zhang, Y.Y. Thermal effects of Qinghai-Tibet highway on permafrost under different surface conditions. *J. Glaciol. Geocryol.* **2022**, *44*, 470–484.